

EXCLUSIVE PHOTO- AND ELECTROPRODUCTION OF MESONS IN THE GEV REGION ^a

G. FOLBERTH, R. ROSSMANN, AND W. SCHWEIGER

*Institute of Theoretical Physics, University of Graz, Universitätsplatz 5,
A-8010 Graz, Austria*

We consider the reactions $\gamma p \rightarrow MB$, with MB being either $K^+ \Lambda$, $K^+ \Sigma^0$, or $\pi^+ n$, within a diquark model which is based on perturbative QCD. The model parameters and the quark-diquark distribution amplitudes of the baryons are taken from previous investigations of electromagnetic baryon form factors and Compton-scattering off protons. Reasonable agreement with the few existing photoproduction data at large momentum transfer is found for meson distribution amplitudes compatible with the asymptotic one ($\propto x(1-x)$). We present also first results for hard electroproduction of the $K^+ \Lambda$ final state. Our predictions exhibit some characteristic features which could easily be tested in forthcoming electroproduction experiments.

1 Introduction

Our investigation of exclusive photo- and electroproduction of mesons is part of a systematic study of hard exclusive reactions^{1,2,3} within a model which is based on perturbative QCD, in which baryons, however, are treated as quark-diquark systems. This model has already been applied to baryon form factors in the space-¹ and time-like region², real and virtual Compton scattering³, two-photon annihilation into proton-antiproton² and the charmonium decay $\eta_c \rightarrow p \bar{p}$ ². A consistent description of these reactions has been achieved in the sense that the corresponding large momentum-transfer data ($p_\perp^2 \gtrsim 3 \text{ GeV}^2$) are reproduced with the same set of model parameters. Further applications of this model include three-body J/Ψ decays⁴ and the calculation of Landshoff contributions in elastic proton-proton scattering⁵. Like the usual hard-scattering approach (HSA)⁶ the diquark-model relies on factorization of short- and long-distance dynamics; a hadronic amplitude is expressed as a convolution of a hard-scattering amplitude \hat{T} , calculable within perturbative QCD, with distribution amplitudes (DAs) ϕ^H which contain the (non-perturbative) bound-state dynamics of the hadronic constituents. The introduction of diquarks does not only simplify computations, it is rather motivated by the requirement to extend the HSA from (asymptotically) large down to intermediate momentum transfers ($p_\perp^2 \gtrsim 3 \text{ GeV}^2$). This is the momentum-transfer region where some experimental data already exist, but where still persisting non-perturbative

^aTalk given by W. Schweiger at the workshop "Diquarks 3", Torino, Italy, Oct. 1996.

effects, in particular strong correlations in baryon wave functions, prevent the pure quark HSA to become fully operational. Diquarks may be considered as an effective way to cope with such effects. Photoproduction of mesons is one class of exclusive reactions where the pure-quark HSA obviously fails in reproducing the hard-scattering data⁷ and where a modification of the perturbative QCD approach seems to be necessary in the few-GeV region.

The following section starts with an outline of the hard-scattering approach with diquarks and introduces the hadron DAs to be used in the sequel. The diquark model predictions for the various reaction channels are presented in Sec. 3 along with some general considerations on photo- and electroproduction reactions. Our conclusions are finally given in Sec. 4.

2 Hard Scattering with Diquarks

Within the hard-scattering approach a helicity amplitude $M_{\{\lambda\}}$ for the reaction $\gamma^{(*)} p \rightarrow M B$ is (to leading order in $1/p_{\perp}$) given by the convolution integral⁶

$$M_{\{\lambda\}}(\hat{s}, \hat{t}) = \int_0^1 dx_1 dy_1 dz_1 \phi^{M\dagger}(z_1, \tilde{p}_{\perp}) \phi^{B\dagger}(y_1, \tilde{p}_{\perp}) \hat{T}_{\{\lambda\}}(x_1, y_1, z_1; \hat{s}, \hat{t}) \phi^p(x_1, \tilde{p}_{\perp}). \quad (1)$$

The distribution amplitudes ϕ^H are probability amplitudes for finding the valence Fock state in the hadron H with the constituents carrying certain fractions of the momentum of their parent hadron and being collinear up to a factorization scale \tilde{p}_{\perp} . In our model the valence Fock state of an ordinary baryon is assumed to consist of a quark (q) and a diquark (D). We fix our notation in such a way that the momentum fraction appearing in the argument of ϕ^H is carried by the quark – with the momentum fraction of the other constituent (either diquark or antiquark) it sums up to 1 (cf. Fig. 1). For our actual calculations the (logarithmic) \tilde{p}_{\perp} dependence of the DAs is neglected throughout since it is of minor importance in the restricted energy range we are interested in. The hard scattering amplitude $\hat{T}_{\{\lambda\}}$ is calculated perturbatively in collinear approximation and consists in our particular case of all possible tree diagrams contributing to the elementary scattering process $\gamma q D \rightarrow q \bar{q} q D$. A few examples of such diagrams are depicted in Fig. 2. The subscript $\{\lambda\}$ represents the set of possible photon, proton and Λ helicities. The Mandelstam variables s and t are written with a hat to indicate that they are defined for vanishing hadron masses. The calculation of the hard scattering amplitude involves an expansion in powers of (m_H/\hat{s}) which is cut off after $\mathcal{O}(m_H/\hat{s})$. Hadron masses, however, are fully taken into account in flux and phase-space factors.

The model, as applied in Refs. 1-3, comprises scalar (S) as well as axial-

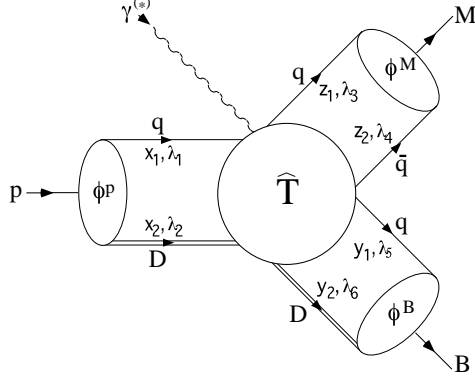


Figure 1: Graphical representation of the hard-scattering formula, Eq. (1), for $\gamma p \rightarrow MB$. x_i , y_i , and z_i denote longitudinal momentum fractions of the constituents, the λ_i 's their helicities.

vector (V) diquarks. V diquarks are important, if one wants to describe spin observables which require the flip of baryonic helicities. The Feynman rules for electromagnetically interacting diquarks are just those of standard quantum electrodynamics. Feynman rules for strongly interacting diquarks are obtained by replacing the electric charge e by the strong coupling constant g_s times the Gell-Mann colour matrix t^a . The composite nature of diquarks is taken into account by multiplying each of the Feynman diagrams with diquark form factors $F_D^{(n+2)}(Q^2)$ which depend on the kind of the diquark ($D = S, V$), the number n of gauge bosons coupling to the diquark, and the square of the 4-momentum Q^2 transferred to the diquark. The form factors are parameterized by multipole functions with the power chosen in such a way that in the limit $p_\perp \rightarrow \infty$ the scaling behaviour of the pure quark HSA is recovered.

Having outlined how diquarks are treated perturbatively, a few words about the choice of the quark-diquark DAs (which incorporate the q-D bound-state dynamics) are still in order. In Refs. 1-3 a quark-diquark DA of the form ($c_1 = c_2 = 0$ for S diquarks, x longitudinal momentum fraction carried by the quark)

$$\phi_D^B(x) \propto x(1-x)^3(1+c_1x+c_2x^2) \exp \left[-b^2 \left(\frac{m_q^2}{x} + \frac{m_D^2}{(1-x)} \right) \right], \quad D = S, V, \quad (2)$$

in connection with an SU(6)-like spin-flavour wave function, turned out to be quite appropriate for octet baryons B. The origin of the DA, Eq. (2), is a nonrel-

$$\begin{aligned}
& \left\{ \text{diagram 1} + \text{diagram 2} - \text{diagram 3} + \dots \right\} \times F_D^{(3)}(-x_2 y_2 t) \\
& \left\{ \text{diagram 4} - \text{diagram 5} + \text{diagram 6} + \dots \right\} \times F_D^{(4)}(-x_2 y_2 t) \\
& \left\{ \text{diagram 7} + \text{diagram 8} + \text{diagram 9} + \dots \right\} \times F_D^{(5)}(-x_2 y_2 t)
\end{aligned}$$

Figure 2: A few representative examples for three-, four-, and five-point contributions to $\gamma p \rightarrow M B$. As indicated, diagrams are first calculated in Born order for point-like diquarks and afterwards multiplied with appropriate vertex functions (diquark form factors).

ativistic harmonic-oscillator wave function⁸. Therefore the masses appearing in the exponential have to be considered as constituent masses (330 MeV for light quarks, 580 MeV for light diquarks, strange quarks are 150 MeV heavier than light quarks). The oscillator parameter $b^2 = 0.248 \text{ GeV}^{-2}$ is chosen in such a way that the full wave function gives rise to a value of 600 MeV for the mean intrinsic transverse momentum of a quark inside a nucleon.

For meson DAs various models can be found in the literature. In order to check the sensitivity of our calculation on the choice of the meson DAs we employ two qualitatively different forms. On the one hand, the asymptotic DA

$$\phi_{\text{asy}}(x) \propto x(1-x), \quad (3)$$

which solves the \tilde{p}_\perp evolution equation for $\phi(x, \tilde{p}_\perp)$ in the limit $\tilde{p}_\perp \rightarrow \infty$, and, on the other hand, the DAs

$$\phi_{\text{CZ}}^\pi(x) \propto \phi_{\text{asy}}(2x-1)^2, \quad \phi_{\text{CZ}}^K(x) \propto \phi_{\text{asy}}[0.08 + 0.6(2x-1)^2 - 0.25(2x-1)^3], \quad (4)$$

which have been proposed in Ref. 9 on the basis of QCD sum rules. The “normalization” of the meson DAs is determined by the experimental decay constants for the weak $\pi, K \rightarrow \mu \nu_\mu$ decays. The analogous constants f_S and f_V for the q-D DAs of baryons are free parameters of the model. They are, in principle, determined by the probability to find the q-D state (D = S, V) in the baryon B and by the transverse-momentum dependence of the corresponding wave function.

For further details of the diquark model we refer to the publication of R. Jakob et al.¹. The numerical values of the model parameters for the present study are also taken from this paper.

3 Photo- and Electroproduction Reactions

Exclusive photoproduction of pseudoscalar mesons can, in general, be described by four independent helicity amplitudes $M_{\lambda_M, \lambda_B, \lambda_\gamma, \lambda_p}$ ¹⁰

$$\begin{aligned} N &= M_{0, -\frac{1}{2}, +1, +\frac{1}{2}}, & S_1 &= M_{0, -\frac{1}{2}, +1, -\frac{1}{2}}, \\ D &= M_{0, +\frac{1}{2}, +1, -\frac{1}{2}}, & S_2 &= M_{0, +\frac{1}{2}, +1, +\frac{1}{2}}. \end{aligned} \quad (5)$$

N , S_1 , S_2 , and D represent non-flip, single-flip, and double-flip amplitudes, respectively. Two additional amplitudes,

$$\tilde{N} = M_{0, +\frac{1}{2}, 0, +\frac{1}{2}}, \quad S_3 = M_{0, -\frac{1}{2}, 0, +\frac{1}{2}}, \quad (6)$$

occur if electroproduction is considered. Electroproduction and photoproduction are related as far as in the one-photon approximation the electroproduction cross section can be expressed in terms of four response functions $d\sigma_U$, $d\sigma_L$, $d\sigma_T$, and $d\sigma_I$ for the production of a pseudoscalar meson by a virtual photon, $\gamma^* p \rightarrow MB$ ¹¹. The two helicity amplitudes in Eq. (6) correspond to the longitudinal polarization degree of the virtual photon. The two response functions $d\sigma_U$ and $d\sigma_L$ are just cross sections for (spin averaged) transversely and longitudinally polarized photons, respectively. The other two functions are transverse-transverse ($d\sigma_T$) and longitudinal-transverse ($d\sigma_I$) interference terms. In the limit of vanishing photon-virtuality ($Q^2 \rightarrow 0$) $d\sigma_U$ reduces to the ordinary photoproduction cross section, the ratio $d\sigma_T/d\sigma_U$ becomes the (negative) photon asymmetry Σ ¹⁰ and $d\sigma_L$ as well as $d\sigma_I$ become zero.

From the q-D flavour functions (D = S, V)

$$\chi_S^p = uS_{[u,d]}, \quad \chi_V^p = [uV_{\{u,d\}} - \sqrt{2}dV_{\{u,u\}}]/\sqrt{3}, \quad (7)$$

$$\chi_S^n = dS_{[u,d]}, \quad \chi_V^n = -[dV_{\{u,d\}} - \sqrt{2}uV_{\{d,d\}}]/\sqrt{3}, \quad (8)$$

$$\chi_S^{\Sigma^0} = [dS_{[u,s]} + uS_{[d,s]}]/\sqrt{2}, \quad \chi_V^{\Sigma^0} = [2sV_{\{u,d\}} - dV_{\{u,s\}} - uV_{\{d,s\}}]/\sqrt{6}, \quad (9)$$

$$\chi_S^\Lambda = [uS_{[d,s]} - dS_{[u,s]} - 2sS_{[u,d]}]/\sqrt{6}, \quad \chi_V^\Lambda = [uV_{\{d,s\}} - dV_{\{u,s\}}]/\sqrt{2}. \quad (10)$$

for the baryons one infers already that the three production channels we are interested in differ qualitatively in the sense that $K^+ \Lambda$ is solely produced via the $S_{[u,d]}$ diquark, $K^+ \Sigma^0$ via the $V_{\{u,d\}}$ diquark, and $\pi^+ n$ via S and V diquarks. An important consequence of this observation is that helicity amplitudes and hence spin observables which require the flip of the baryonic helicity are predicted to vanish for the $K^+ \Lambda$ final state (e.g., the polarization P of the outgoing Λ). For the other two channels helicity flips may, of course, take place by means of the V diquark.

One of the qualitative features of the HSA is the fixed-angle scaling behaviour of cross sections. The pure quark HSA implies an s^{-7} decay of the photoproduction cross section. This scaling behaviour is, of course, recovered within the diquark model in the limit $s \rightarrow \infty$. However, at finite s , where the diquark form factors become operational and diquarks appear as nearly elementary particles, the s^{-7} power-law is modified. Additional deviations from the s^{-7} decay of the cross section are due to logarithmic corrections which have their origin in the running coupling constant α_s and eventually in the evolution of the DAs ϕ^H (neglected in our calculation).

3.1 The $K^+ - \Lambda$ Channel

Figure 3 (left) shows the diquark-model predictions for the (scaled) photoproduction cross section $s^7 d\sigma/dt$ along with the few existing photoproduction data at large-momentum transfer¹² and the outcome of the pure quark HSA⁷ (dash-dotted curve). Whereas the DAs of proton and Λ have been kept fixed according to Eq. (2) we have varied the K^+ DA. The solid and the dashed line represent results for the asymptotic (Eq. (3)) and the two-humped (Eq. (4)) K^+ DA, respectively, evaluated at $p_{\text{lab}}^\gamma = 6$ GeV. The better performance of the asymptotic DA and the overshooting of the asymmetric DA is in line with the conclusion drawn from the investigation of the pion-photon transition form factor¹⁴ where, for the case of the pion, ϕ_{CZ}^π leads also to an overshooting the data. Our findings have to be contrasted with those obtained within the pure quark-model calculation of photoproduction⁷, where the asymptotic forms for both, baryon and meson DAs, give systematically larger results than the combination of very asymmetric DAs. However, the numerics of Ref. 7 must be taken with some proviso. For Compton scattering off nucleons it has been demonstrated¹⁵ that the very crude treatment of propagator singularities adopted in Ref. 7, namely keeping $i\epsilon$ small but finite, may lead to deviations from the correct result which are as large as one order of magnitude. At this point we want to emphasize that we have paid special attention to a correct and numerically robust treatment of the propagator singularities which occur in the convolution integral, Eq. (1). By carefully separating the singular contributions, exploiting delta functions, rewriting principal-value integrals as ordinary integrals plus analytically solvable principle-value integrals, we are able to do all the numerical integrations by means of very fast and stable fixed-point Gaussian quadratures.

We have also examined the relative importance of various groups of Feynman graphs and found the 3-point contributions to be by far the most important (cf. Fig. 3 (left)). 4- and 5-point contributions amount to $\approx 5\%$

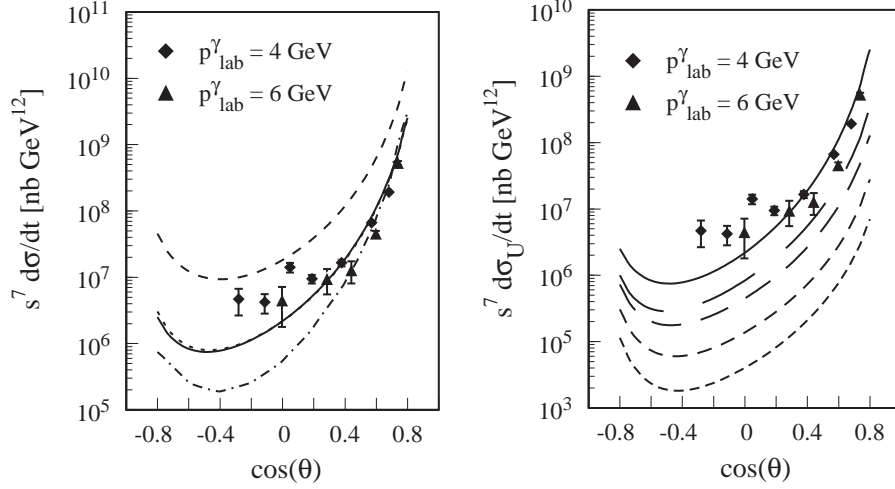


Figure 3: Diquark-model predictions for photo- (left figure) and electroproduction (right figure) of the $K^+\Lambda$ final state. Results are shown for fixed $p_{\text{lab}}^\gamma = 6$ GeV. The experimental points are photoproduction data taken from Anderson et al.¹². *Left figure*: differential cross section for $\gamma p \rightarrow K^+ \Lambda$ scaled by s^7 vs $\cos(\theta_{\text{cm}})$; solid (dashed) line: diquark-model result for p and Λ DAs chosen according to Eq. (2), K^+ DA according to Eq. (3) (Eq. (4)); dotted line: same as full line, but only three-point contributions taken into account; dash-dotted line: quark-model result⁷ for the asymmetric p and Λ DAs of Ref. 13 and the two-humped K^+ DA of Eq. (4). *Right figure*: the spin-averaged cross section $d\sigma_U/dt$ (scaled by s^7) vs $\cos(\theta_{\text{cm}})$ for transversely polarized photons with virtualities $Q^2 = 0$ (photoproduction limit), 0.5, 1, 2, and 3 GeV^2 ; dashes become shorter with increasing Q^2 . Proton and Λ DAs are chosen according to Eq. (2), the K^+ DA according to Eq. (3).

at $\theta_{\text{cm}} = 90^\circ$ and $E_{\text{lab}}^\gamma = 6$ GeV as long as only $d\sigma/dt$ is considered. Spin observables, on the other hand, are much more affected by 4- and 5-point contributions. A more detailed discussion of $\gamma p \rightarrow K^+ \Lambda$ (and also $\gamma p \rightarrow K^{*+} \Lambda$) with a full account of calculational techniques and analytical expressions for the photoproduction amplitudes can be found in Ref. 16.

The diquark-model predictions for a few electroproduction observables are depicted in Fig. 3 (right) and Fig. 4. In these plots we have concentrated on the asymptotic form, Eq. (3), of the K^+ DA. Like in the case of photoproduction the large- s behaviour of the four cross section contributions is s^{-7} (modified by logarithmic factors) provided that Q^2/s is kept fixed. For fixed photon virtuality Q^2 and $s \rightarrow \infty$, however, $d\sigma_L/dt$ and $d\sigma_T/dt$ decay like s^{-9} and s^{-8} , respectively. For fixed $p_{\text{lab}}^\gamma = 6$ GeV the transverse cross-section contribution $d\sigma_U/dt$ decreases with increasing Q^2/s (cf. Fig. 3 (right)). The same holds for

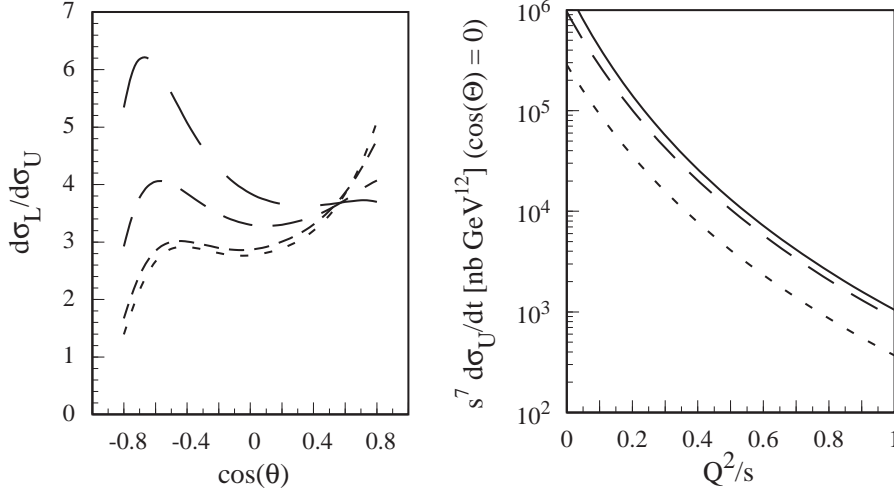


Figure 4: Diquark-model predictions for electroproduction of the $K^+\Lambda$ final state. *Left figure:* ratio of cross sections $d\sigma_L/d\sigma_U$ for longitudinally and transversely polarized photons, respectively, vs $\cos(\theta_{\text{cm}})$ for fixed $p_{\text{lab}}^\gamma = 6$ GeV; dashes become shorter with increasing photon virtuality Q^2 ($= 0.5, 1, 2, 3$ GeV²). *Right figure:* $d\sigma_U/dt$ at fixed $\theta_{\text{cm}} = 90^\circ$ vs Q^2/s for $s = 10$ (solid), 20 (long dashed), and 100 GeV² (short dashed).

$d\sigma_L/dt$ (if $Q^2/s \gtrsim 0.04$). At $Q^2/s = 0.04$ $d\sigma_L/dt$ is already larger than $d\sigma_U/dt$ (cf. Fig. 4 (left)). Since $d\sigma_L/dt$ vanishes for $Q^2 \rightarrow 0$ it thus has to rise very sharply at small values of Q^2/s . To get a better feeling for the Q^2 -dependence of $d\sigma_U/dt$ we have plotted this quantity for fixed scattering angle ($\theta_{\text{cm}} = 90^\circ$) and different values of s as function of Q^2/s (cf. Fig. 4 (right)). For exact s^{-7} scaling the curves for the three different values of s should coincide. The deviation from the s^{-7} scaling can mainly be ascribed to the running coupling constant α_s . The dependence of $d\sigma_U/dt$ (and likewise $d\sigma_L/dt$) on Q^2/s can be roughly parameterized by means of a function $\propto (1 + cQ^2/s)^{-6}$ with the parameter c between 2 and 2.5. The qualitative features, like scaling behaviour, Q^2/s dependence, and dominance of $d\sigma_L/dt$ as compared to $d\sigma_U/dt$ remain, of course, unaltered if the asymptotic K^+ DA is replaced by the asymmetric DA of Eq. (4). The angular dependence of cross-section ratios, like $d\sigma_L/d\sigma_U$, $d\sigma_T/d\sigma_U$, or $d\sigma_1/d\sigma_U$, however, exhibit a marked sensitivity on the choice of the K^+ DA. First experimental constraints on hard exclusive electroproduction are to be expected from CEBAF and later on at even higher momentum transfers from ELFE (at DESY).

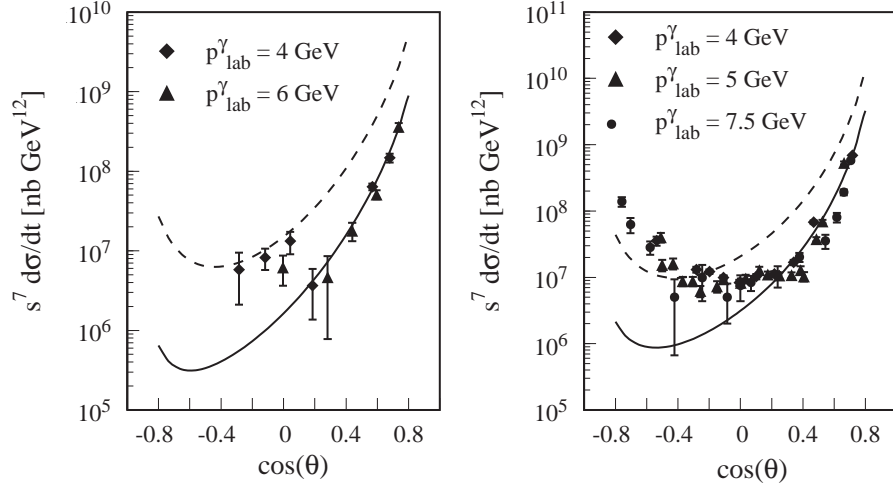


Figure 5: Diquark-model predictions for photoproduction of the $K^+-\Sigma^0$ (*left figure*) and the π^+-n (*right figure*) final states; solid (dashed) line: diquark-model results for baryon DAs chosen according to Eq. (2), K and π DAs according to Eq. (3) (Eq. (4)). Results are shown for fixed $p_{\text{lab}}^\gamma = 6 \text{ GeV}$. Scalar-diquark contributions are fully taken into account, four- and five-point contributions of vector diquarks are neglected. Data are taken from Anderson et al.¹².

3.2 *The $K^+-\Sigma^0$ and the π^+-n Channel*

We have already mentioned that these channels differ from $K^+-\Lambda$ production as far as also V-diquarks are involved. Since the treatment of V diquarks is much more intricate than that of S diquarks we have, until now, only calculated the corresponding three-point contributions. From $K^+-\Lambda$ production and also from other applications of the diquark model we know, however, that spin-averaged cross sections are mainly determined by three-point contributions. Thus we do not expect a significant modification of our numerical results for the $K^+-\Sigma^0$ and the π^+-n photoproduction cross sections if four- and five-point contributions of V diquarks are included. Like in the case of $K^+-\Lambda$ production we observe reasonable agreement with the $K^+-\Sigma^0$ and the π^+-n cross-section data if the asymptotic DA is taken for the K^+ and the π^+ , respectively (cf. Fig. 5). The two-humped DAs, Eq. (4), seem again to be in conflict with the data. Also for these two channels the pure quark HSA fails in reproducing the data. It is remarkable that the unpolarized differential cross sections for $K^+-\Lambda$ and $K^+-\Sigma^0$ production are very similar in size, although the corresponding production mechanisms (via S and V diquarks, respectively) are quite different. We expect this difference to show up more clearly in spin observables.

4 Conclusions

The predictions of the diquark model for $\gamma p \rightarrow K^+ \Lambda$, $K^+ \Sigma^0$, and $\pi^+ n$ look rather promising if the asymptotic form ($\propto x(1-x)$) is taken for the meson DAs. To the best of our knowledge the diquark model is, as yet, the only constituent scattering model which is able to account for the large- p_\perp photoproduction data. For electroproduction of the $K^+ \Lambda$ final state our results are the first perturbative QCD predictions at all. With respect to future experiments it would, of course, be desirable to have more and better large momentum-transfer data on exclusive photo- and electroproduction. Polarization measurements of the recoiling particle could help to decide, whether the perturbative regime has been reached already, or whether non-perturbative effects (different from diquarks) are still at work. Spin observables, in general, could be very helpful to constrain the form of the hadron DAs.

References

1. R. Jakob, P. Kroll, M. Schürmann, and W. Schweiger, *Z. Phys. A* **347**, 109 (1993).
2. P. Kroll, Th. Pilsner, M. Schürmann, and W. Schweiger, *Phys. Lett. B* **316**, 546 (1993).
3. P. Kroll, M. Schürmann, and P. A. M. Guichon, *Nucl. Phys. A* **598**, 435 (1996).
4. E.-H. Kada and J. Parisi, *Z. Phys. C* **70**, 303 (1996).
5. R. Jakob, *Phys. Rev. D* **50**, 5647 (1994).
6. See, e.g., S. J. Brodsky and G. P. Lepage in *Perturbative Quantum Chromodynamics*, ed. A. H. Mueller (World Scientific, Singapore, 1989).
7. G. R. Farrar, K. Huleihel, and H. Zhang, *Nucl. Phys. B* **349**, 655 (1991).
8. T. Huang, *Nucl. Phys. [Proc. Suppl.] B* **7**, 320 (1989).
9. V. L. Chernyak and A. R. Zhitnitsky, *Phys. Rep.* **112**, 173 (1984).
10. I. S. Barker, A. Donnachie, and J. K. Storrow, *Nucl. Phys. B* **95**, 347 (1975).
11. R. C. E. Devenish and D. H. Lyth, *Phys. Rev. D* **5**, 47 (1972).
12. R. L. Anderson et al., *Phys. Rev. D* **14**, 679 (1976).
13. G. R. Farrar, H. Zhang, A. A. Ogloblin, and I. R. Zhitnitsky, *Nucl. Phys. B* **311**, 585 (1988).
14. R. Jakob, P. Kroll, and M. Raulfs, *J. Phys. G* **22**, 45 (1996).
15. A. S. Kronfeld and B. Nižič, *Phys. Rev. D* **44**, 3445 (1991).
16. P. Kroll, M. Schürmann, K. Passek, and W. Schweiger, preprint UNIGRAZ-UTP 15-04-96 (hep-ph/9604353), to appear in *Phys. Rev. D*.